ACS APPLIED MATERIALS & INTERFACES

Letter

www.acsami.org

Vertically Ordered Hematite Nanotube Array as an Ultrasensitive and Rapid Response Acetone Sensor

Do Hong Kim,[†,‡] Young-Seok Shim,[†] Jong-Myeong Jeon,[†] Hu Young Jeong,[§] Sung Soo Park,[⊥] Young-Woon Kim,[†] Jin-Sang Kim,[∥] Jong-Heun Lee,*[,‡] and Ho Won Jang*[,†]

[†]Department of Materials Science Engineering, Research Institute of Advanced Materials, Seoul National University, Seoul 151-744, Korea

[‡]Department of Materials Science Engineering, Korea University, Seoul 136-713, Korea

[§]UCRF and [⊥]School of Materials Science and Engineering, Ulsan National Institute of Science and Technology, Ulsan 689-798, Korea

[∥]Electronic Materials Research Center, Korea Institute of Science and Technology, Seoul 136-791, Korea

Supporting Information

ABSTRACT: Vertically ordered nanotube array is a desirable configuration to improve gas sensing properties of the hematite which is the most abundant and cheapest metal oxide semiconductor on earth but has low and sluggish chemiresistive responses. We have synthesized a vertically aligned, highly ordered hematite nanotube array directly on a patterned SiO_2/Si substrate and then it used as a gas sensor without additional processing. The nanotube array sensor shows unprecedentedly ultrahigh and selective responses to acetone with detection limits down to a few parts per billion and response time shorter than 3 s.

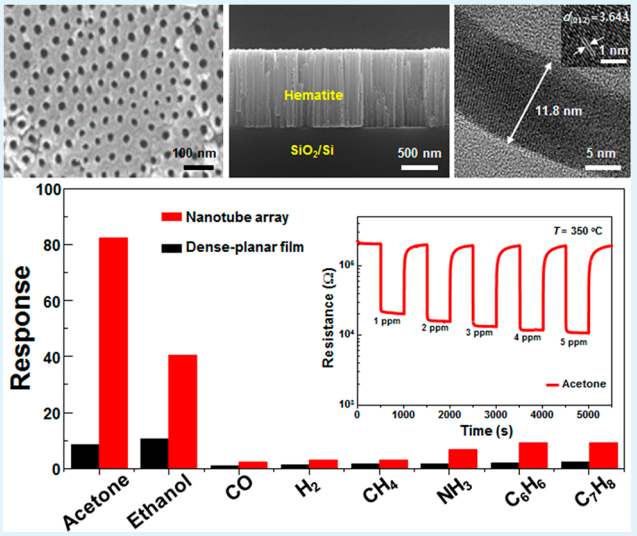

KEYWORDS: *hematite, nanotube array, acetone sensor, earth abundant, ultrasensitive*

Semiconducting metal oxide gas sensors have considerable interests in diverse applications such as environmental monitoring, agriculture, medical diagnosis, aerospace industries, and mobile applications because of their small size, low cost, and simplicity in operation.,[1,2] various oxide materials including SnO_2, WO_3, ZnO_2, and TiO_2, have so far been studied. Beside them, hematite (α-Fe_2O_3), one of the most stable iron oxide forms, has been identified as a promising candidate as a gas sensing material since it is a chemically stable n-type semiconductor with the band gap energy of 2.2 eV. More importantly, hematite is the most abundant and cheapest semiconductor metal oxide which we can be obtain on earth. According to the U.S. Geological Institute, the world mineral resources of iron are estimated to exceed 800 billion tonnes (Figure 1a).[3] The annual world production of iron was reported up to 3.1 billion tonnes in 2012 (Figure 1b). This value is approximately 4 orders of magnitude higher than the annual production of Sn from which the oxide SnO_2 is most widely used for gas sensors. Nevertheless, gas sensors based on hematite have been rarely explored for the detection of a variety of gases due to their low sensitivities and sluggish response compared with gas sensors based on SnO_2.[4,5]

It is well-known that nanostructure possesses high surface-to-volume ratio, increased surface activity, and strong adsorption/desorption ratio of the target gas molecules, so the metal oxide nanostructures are expected to excellent gas sensing performance.[6,7] For instance, gas sensors based on one-dimensional metal oxide nanostructures such as nanowires, nanorods, nanobelts, and nanotubes, have been widely exploited for gas sensor application. However, low-cost and high yield mass production of one-dimensional metal oxide materials as gas sensors remains still challenging. Vertically ordered nanotubes prepared by facile anodic oxidation of metal are considered as a promising configuration for gas sensors. Particularly, extremely

Received: June 29, 2014
Accepted: August 26, 2014
Published: August 26, 2014

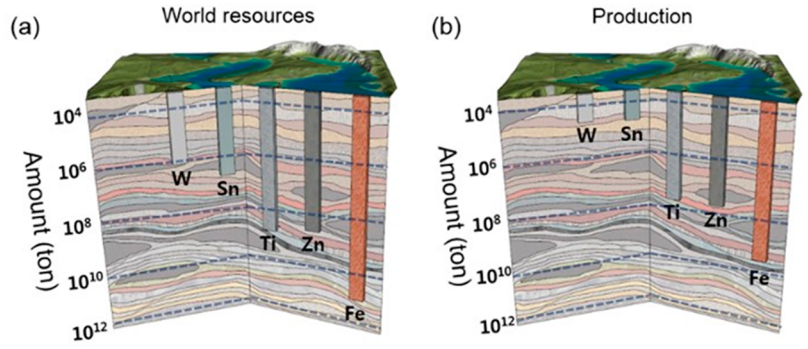

Figure 1. (a) World mineral resources on earth and (b) world production on 2012 for W, Sn, Ti, Zn, and Fe. Data for the plots were extracted from Mineral Commodity Summaries 2013 provided by U.S. Geological Survey.[3]

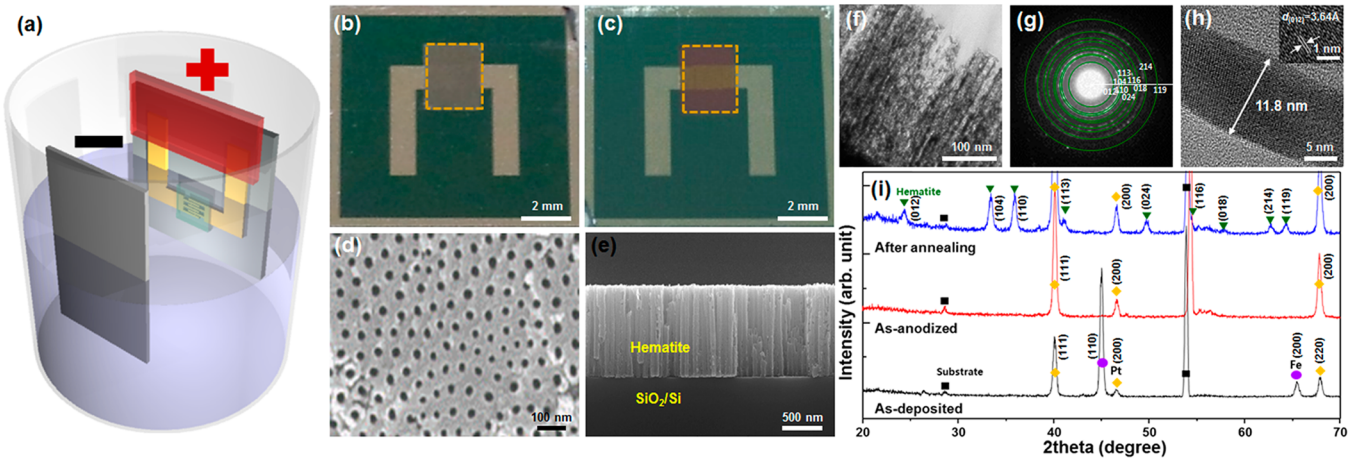

Figure 2. (a) Sketch illustrating our anodization method to form Fe_2O_3 nanotube array on Pt-IDEs-patterned SiO_2/Si substrate. The Key idea of our method is clamping the Pt electrodes as the current spreader during anodization. (b, c) Photographs of a Fe film on Pt-patterned SiO_2/Si substrate (b) before anodization and (c) after anodization. (d) Plain-view SEM images of Fe_2O_3 nanotube array on Pt-IDEs-patterned SiO_2/Si substrate. (e) High magnification cross-sectional SEM images of the Fe_2O_3 nanotube array. (f) Cross-sectional TEM image of hematite nanotube array. (g) Selected area diffraction pattern with indexing. (h) High-magnification TEM image of the wall thickness of a hematite nanotube. The inset shows the interplanar spacing of 0.364 nm corresponding to a (012) plane. (i) Glancing angle X-ray diffraction patterns of a Fe/Pt/SiO_2/Si structure before anodization and Fe_2O_3 nanotube arrays before and after annealing at 550 °C for 5 h.

large specific surface area compared with dense planar film counterparts provides excellent adsorption and desorption of gas molecules, which is desirable for high-performance gas sensors.

To date, the synthesis of hematite nanotubes has relied on hydrothermal,[8] template-assisted,[9] and electrochemical anodization methods.[10] Hydrothermal synthesis is a simple method to prepare nanotubular structures, but typically involves harsh chemical conditions such as low or high pH which leads to substrate damage. In addition, because the synthesized hematite nanotubes are composed of randomly distributed, the intrinsic large surface area of hematite nanotubes cannot be fully utilized for gas sensing. Template-assisted method using anodic aluminum oxide (AAO) has been a simple synthetic route to prepare nanotubular structures. However, the AAO templating is not compatible with high throughput semiconductor fabrication processes. The anodization of Fe foils can lead to hematite nanotubes. However, the anodization of Fe foils has not been exploited for chemiresistive gas sensors since the remained Fe foils beneath the nanotubes easily form electrical shorts with the sensor electrodes. In addition, the concurrent oxidation of the underlying Fe foils at elevated temperatures hinders reliable gas sensing performance. Alternatively, the most attractive approach is the direct synthesis of vertically ordered hematite nanotubes on patterned SiO_2/Si substrates through electrochemical anodization. However, no work has been reported on the synthesis of hematite nanotubes on a foreign substrate because there are some difficult problems to be solved. Usually, the quality of metal oxide nanotube array obtained by the anodization of a metal film on a foreign substrate is worse than that by the anodization of a free-standing metal foil.[11−13] The clamped area for electrical contact remains unanodized. In addition, the complete anodization of Fe into Fe_2O_3 is hard to be achieved owing to the occurrence of potential gradients in the Fe film during anodization. The key idea of our anodization method to achieve the complete anodization of the whole area of Fe film into Fe_2O_3 nanotube array is the use of Pt bottom electrodes as the current spreader for anodization. This strategy has not been applied to the synthesis of a hematite nanotube array.

Recently, selective acetone sensing attracts interests for the application in the diagnosis of diabetes from human exhaled breath.[14] For semiconducting metal oxide gas sensors, selective acetone sensing against interfering gases such as ethanol and toluene have been achieved mainly using the optimization of the operating temperatures.[15] Here, we report that a vertically ordered hematite nanotube array on a patterned SiO_2/Si substrate can be utilized as a selective acetone sensor. The

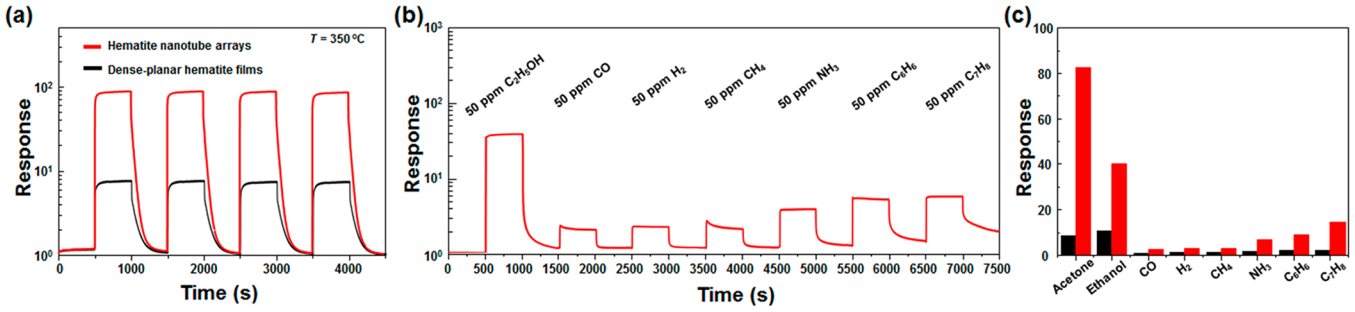

Figure 3. (a) Dynamic sensing transients of the dense-planar hematite films and hematite nanotube array to 50 ppm acetone at 350 °C. (b) Sensing transients of the hematite nanotube array to various gases. (c) Response of dense-planar hematite films and the hematite nanotube array to various gases.

direct synthesis of a hematite nanotube array on SiO_2/Si substrates patterned with Pt electrodes leads to ultrasensitive and selective sensors to acetone., In additional, the 90% response time of the hematite nanotube sensor is ∼3 s, which is much shorter than that of the dense-planar hematite film, suggesting the potential use of the hematite nanotube sensor for the noninvasive diagnosis of human diabetes.

Figure 2a shows a sketch illustrating our anodization method to form a hematite nanotube array with Pt IDEs used in this study. The details of the experimental methods are described in the Supporting Information. The key idea of our method to accomplish the complete anodization of the whole area of the Fe film into Fe_2O_3 nanotube array is clamping the Pt IDEs rather than the Fe film itself for the anodization. By clamping the Pt IDEs which cannot be anodized, the current efficiently spreads though the underlying Pt IDEs to the Fe film, potential gradients do not establish within the Fe film, resulting in the uniform anodization of Fe to Fe_2O_3. In particular, when the thickness of the remaining Fe film is very thin, the current flow through Pt IDEs to the Fe film is still effective, leading to the complete anodization of the Fe film without unconverted regions. We found that the quality of the initial Fe film is critical for the formation of vertically ordered nanotube array. When the Fe film was deposited at 400 °C, the film was observed to be highly textured with columnar grains (see the Supporting Information, Figure S1). Vertically ordered Fe_2O_3 nanotube array could be obtained from the anodization of the Fe film deposited at 400 °C. The photographs in Figure 2b, c show that the Fe film was converted to semitransparent reddish Fe_2O_3 after anodization. The plain-view SEM image in Figure 2d shows the Fe_2O_3 nanotube array formed on a Pt-IDE-patterned SiO_2/Si substrate. By cross-sectional SEM, we have confirmed that the Fe film was completely converted to Fe_2O_3 nanotube array by SEM. The synthesized Fe_2O_3 nanotube array was vertical and unprecedentedly highly ordered with uniform diameters of ∼70 nm as shown in Figure 2e. This result indicates that vertically ordered Fe_2O_3 nanotube array could be directly synthesized on SiO_2/Si substrate using the present anodization method. To the best of our knowledge, no previous studies have been published for direct synthesis of a highly ordered hematite nanotube array on a foreign substrate.

The TEM image in Figure 2f shows that the nanotube array is vertically ordered with uniform diameters. The selected area electron diffraction (SAED) pattern (Figure 2g) confirms again the polycrystalline characteristics of the Fe_2O_3 nanotube array after annealing at 550 °C. The SAED pattern could be indexed as the pure hematite phase of Fe_2O_3 with lattice constants of a = 5.0345 Å, and c = 13.7524 Å (JCPDS#87−1164). The high-resolution TEM image (Figure 2h) reveals that a hematite nanotube array is faceted with a (012) plane with the interplanar spacing of 0.364 nm. It reveals that the wall thickness is ∼12 nm, indicating that the inner diameter of the nanotube is about 50 nm. The XRD patterns of a Fe film and Fe_2O_3 nanotube array before and after annealing at 550 °C are presented in Figure 2i. No metallic Fe peak was observed from the as-anodized nanotube array, which confirms the complete conversion of the Fe film to Fe_2O_3 nanotube array. Because the as-anodized Fe_2O_3 nanotube array is amorphous, no diffraction peaks are observed. After annealing, the Fe_2O_3 nanotube array showed sharp peaks corresponding to the hematite phase without secondary phases.

A typical response curve of the hematite nanotube array to 50 ppm acetone at 350 °C is shown in Figure 3a. The response, S, is defined as $R_{ambient}/R_{gas}$ for the reducing gases (acetone, ethanol, CO, H_2, C_6H_6, C_7H_8, NH_3, and CH_4) where R_{gas} and $R_{ambient}$ denote resistances in the presence and the absence of a test gases, respectively. Upon exposure to acetone, the hematite nanotube array quickly responded with a decrease in resistance, which revealed the typical n-type semiconducting behavior of the hematite nanotube array. Compared with the reference sensor based on a dense-planar hematite film (see the Supporting Information, Figure S2), the hematite nanotube array exhibits about 10 times higher responses to 50 ppm acetone. The gas sensing mechanism of the hematite nanotube array can be explained by the surface-depletion model.[16] When the hematite nanotube array is exposed to dry air, oxygen ions are adsorbed onto the hematite nanotube surface. Therefore, the depletion layer may extend throughout the whole area of the hematite nanotube array, which leads to high resistance. On the other hands, upon exposure to reducing gas such as acetone, gas molecules will react with the chemisorbed oxygen ions at the hematite nanotube surface to form CO_2 and H_2O (as shown in eqs 1 and 2). This increases the charge carrier concentration in the hematite nanotube walls and narrows the surface depletion layer width, which leads to decrease in the resistance of the hematite nanotube array (see the Supporting Information, Figure S3).

$$O_2(g) + 2e^- \rightarrow 2O^-(ads) \quad (1)$$

$$CH_3COCH_3(ads) + 8O^-(ads) \rightarrow 3CO_2(g) + 3H_2O(l) + 8e^- \quad (2)$$

The maximum response of acetone is as high as 84, which is much higher those of previously reported for high sensitivity sensors based on hematite nanotubes, porous hematite,

dx.doi.org/10.1021/am504156w | ACS Appl. Mater. Interfaces 2014, 6, 14779−14784

Table 1. Gas Responses of Different Hematite Nanostructures to Various Gases, As Reported in the Literature and the Present Study

sensing materials	method	conc. (ppm)	$S_{acetone}$	$S_{ethanol}$	$S_{ammonia}$	S_{CO}	$S_{benzene}$	$S_{toluene}$	$S_{hydrogen}$	$S_{methane}$	T_{sens}(°C)	ref
α-Fe_2O_3 NTs	anodization	50	84	40.2	9.5	4.2	10.7	18.6	5.1	5.6	350	in this study
α-Fe_2O_3 NTs	AAO templating method	50		27					2.25		RT	9
α-Fe_2O_3 NTs	hydrothermal	20	15	7	2.5						270	17
		2000	110	42	17							17
Pt-doped α-Fe_2O_3 spheres	solvothermal	100		2.55							400	18
porous α-Fe_2O_3	hydrothermal	1000	92	124								19
porous α-Fe_2O_3 spheres	hydrothermal	50		6.8							260	20
spherelike α-Fe_2O_3 nanocrystal	solvothermal	400		79.7								21
α-Fe_2O_3 nanoparticles	solid-stat chemical reaction	100	22.4	21.1							270, 255	22
Sn-doped wheat sheaflike α-Fe_2O_3	hydrothermal	100		8.8							250	23
hollow α-Fe_2O_3 polyhedras	hydrothermal	500		42.5							270	24
porous Au/α-Fe_2O_3	hydrothermal	500	78.3								300	25
urchinlike α-Fe_2O_3	hydrothermal	100	10	12							260, 275	26
X-shaped α-Fe_2O_3 crystal	hydrothermal	250				1.85	1.95				300	27
urchinlike Ag/α-Fe_2O_3 spheres	hydrothermal	200	75.1	55.2							350	28
α-Fe_2O_3 hollow spheres	hydrolysis process	100		27		1.7	5				300	29
bundlelike α-Fe_2O_3 nanorods	hydrothermal	100	38.5	26.8				7.8			250	30

hematite spheres, nanocrystals, nanoparticles, and nanorods (Table 1).[9,17−30] This exceptional response of the hematite nanotube array is attributed to the porous nanostructure with high surface-to-volume ratio. To identify the selectivity of the hematite nanotube array to acetone, we measured responses to various gases such as ethanol, CO, H_2, CH_4, NH_3, C_7H_8, and C_6H_6 at 350 °C as shown in Figure 3b. Evidently, the hematite nanotube array displays the highest sensitivity to acetone. Fe_2O_3 is known to accelerate the oxidation (or combustion) of gases containing methyl groups such as acetone (methyl−methyl ketone), methanol (methyl alcohol) and butatone (methyl−ethyl ketone) at elevated temperatures under oxidizing atmosphere.[31,32] The large surface area of the hematite nanotube array promotes the reported oxidation of acetone. Thus, the hematite nanotubes themselves has been used as catalysts to oxidize acetone to the final products, CO_2 and H_2O. Therefor the excellent sensitivity for acetone can be attributed to the catalytic role of hematite nanotube to promote the oxidation of methyl groups. For comparison, Figure 3c presents a bar graph of the responses of dense planar hematite films and hematite nanotube array toward eight interference gases at a concentration of 50 ppm. Compared to reference dense planar hematite films, the hematite nanotube array shows higher response to various gases. We can clearly identify that the hematite nanotube array showed the highest sensitivity and selectivity toward acetone gas as opposed to any other gas. To find the optimal sensing temperatures for acetone and ethanol gases, responses of the hematite nanotube array to 50 ppm acetone and ethanol were measured at temperatures ranging from 300 to 450 °C, as shown in Figure 4a. First of all, the hematite nanotube array shows highest response to acetone at 350 °C. The response ratio, $S_{acetone}/S_{ethanol}$, is higher than 2.1. Not only supreme sensitivity, the hematite nanotube array also exhibits extremely high selectivity to acetone at the temperature. As shown in Figure 4b, the 90% response time of the hematite nanotube array is about 3 s, which is much shorter than that of the dense-planar hematite film (28 s, see the Supporting Information, Figure S4). To evaluate the detection limits of the hematite nanotube array to acetone, we measured the response curves of the hematite nanotube array to 1−5 ppm acetone at 350 °C. The responses of the hematite nanotube array are 10.28, 13.21, 15.6, 17.7, and 20.1 to 1, 2, 3, 4, and 5 ppm acetone. Although the 0.5 ppm concentration was the lowest experimentally examined in the present study, the theoretical detection limit (signal-to-noise ratio >3)[33] is calculated to be approximately 1.71 ppb for acetone (Figure 4c, see the Supporting Information for details). Detection limits of subppb levels to acetone demonstrate the potential of the sensor for use in high performance acetone sensors. Because acetone is found in the breath of patients with diabetes mellitus (acetone 0.1−10 ppm),[15] we suggest that the hematite nanotube array synthesized by anodization is very promising for use in high-quality sensor materials for breath analyzers to diagnose diabetes mellitus. Figure 4d shows the change of response of the hematite nanotube array to 50 ppm acetone for 48 days. During the test, the hematite nanotube array repeatedly recovered its original base resistance. Furthermore, the hematite nanotube array could be subjected to long-term operation without degradation.

In summary, we have developed an effective and viable anodization method to obtain highly ordered and uniform hematite nanotube array for sensor application. Using the method, a vertically ordered hematite nanotube array could be directly synthesized on patterned Si substrates and then used for gas sensors without additional process. Our hematite nanotube array displayed ultrahigh and selective responses to acetone with detection limits down to a few parts per billion and response time shorter than 3 s. Excellent selectivity and ppb-level detection limits toward acetone demonstrate the promising potential of the hematite nanotubes for breath

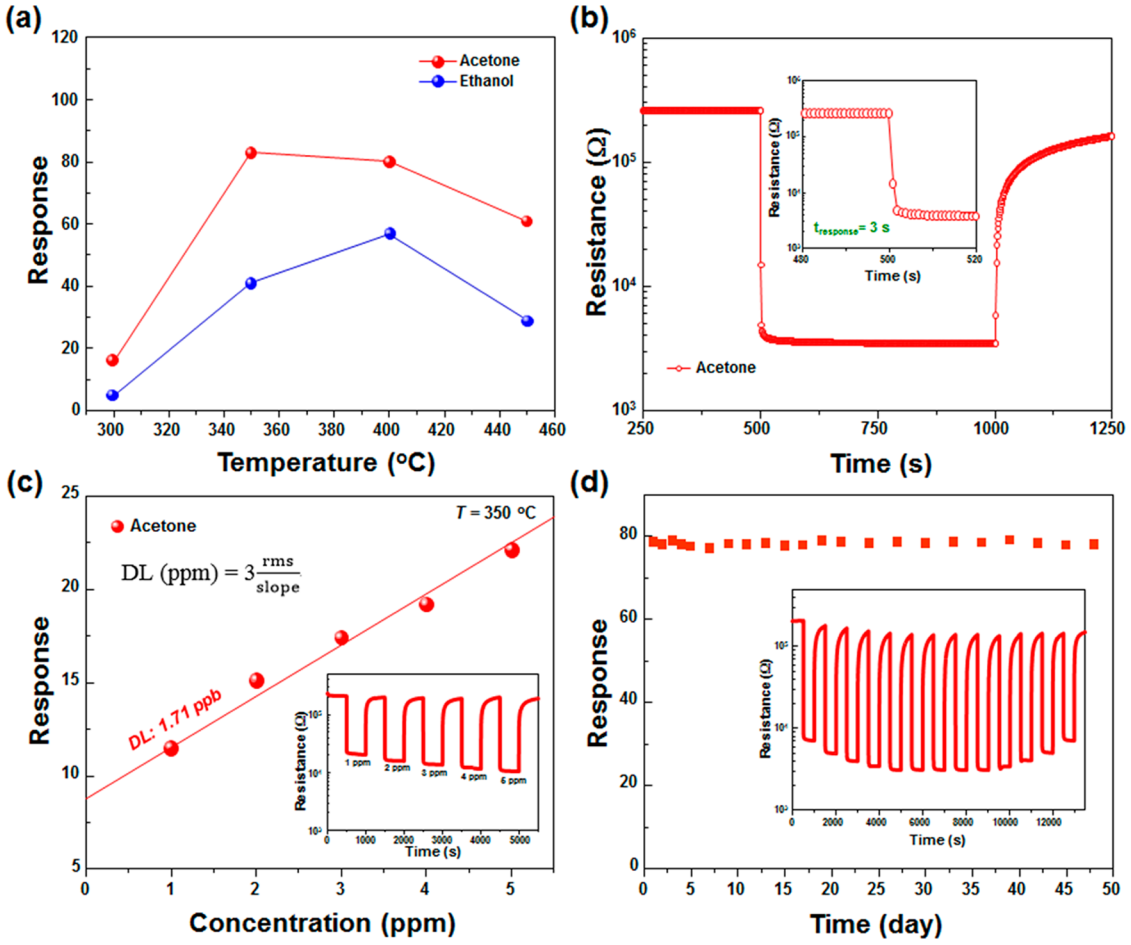

Figure 4. (a) Responses of the hematite nanotube array to 50 ppm acetone and ethanol as a function of temperature. (b) Dynamic acetone sensing transient of hematite nanotube array at 350 °C. Inset: 90% response time ($t_{response}$) of the hematite nanotube array. (c) Theoretical detection limits (DL) of hematite nanotube array to acetone. Inset: response curve of the hematite nanotube array to 1−5 ppm acetone at 350 °C. (d) Change of response of hematite nanotube array to 50 ppm acetone for 48 days. Inset: response to 13 consecutive pulses of 10−50 ppm acetone after 48 days of operation.

analysers to diagnose diabetes mellitus. Furthermore, highly aligned hematite nanotube array with high surface area to volume ratio can open new energy and environment applications including solar cells, water splitting cells, batteries, CO_2 conversion cells, and water purification membranes.

■ ASSOCIATED CONTENT

Ⓢ Supporting Information

Detailed information about the sensor fabrication, characterization, sensor measurements, calculation of theoretical detection limits, morphologies and 90% response time of the hematite nanotube array and the dense-planar hematite film, and the gas sensing mechanism of the hematite nanotube array sensor.. This material is available free of charge via the Internet at http://pubs.acs.org.

■ AUTHOR INFORMATION

Corresponding Authors

*E-mail: jongheun@korea.ac.kr.
*E-mail: hwjang@snu.ac.kr.

Notes

The authors declare no competing financial interest.

■ ACKNOWLEDGMENTS

This work was financially supported by the Center for Integrated Smart Sensors funded by the Ministry of Science, ICT & Future Planning as the Global Frontier Project, the Outstanding Young Researcher Program through the National Research Foundation of Korea, the Aspiring Researcher Program through Seoul National University in 2013, and a research program of the Korea Institute of Science and Technology.

■ REFERENCES

(1) Yamazoe, N.; Shimanoe, K. Proposal of Contact Potential Promoted Oxide Semiconductor Gas Sensor. *Sens. Actuators, B* **2013**, *187*, 162−167.
(2) Hwang, I. S.; Kim, Y. S.; Kim, S. J.; Ju, B. K.; Lee, J. H., A Facile Fabrication of Semiconductor Nanowires Gas Sensor using PDMS Patterning and Solution Deposition. *Sens. Actuators, B 136* (1), 224−229.
(3) http://www.usgs.gov/, accessed on 29 May 2014.
(4) Liao, L.; Zheng, Z.; Yan, B.; Zhang, J. X.; Gong, H.; Li, J. C.; Liu, C.; Shen, Z. X.; Yu, T. Morphology Controllable Synthesis of alpha-Fe_2O_3 1D Nanostructures: Growth Mechanism and Nanodevice Based on Single Nanowire. *J. Phys. Chem. C* **2008**, *112*, 10784−10788.
(5) Wu, Z. C.; Yu, K.; Zhang, S. D.; Xie, Y. Hematite Hollow Spheres with a Mesoporous Shell: Controlled Synthesis and Applications in

Gas Sensor and Lithium Ion Batteries. *J. Phys. Chem. C* **2008**, *112*, 11307−11313.
(6) Pan, X. F.; Liu, X.; Bermak, A.; Fan, Z. Y. Self-Gating Effect Induced Large Performance Improvement of ZnO Nanocomb Gas Sensors. *ACS Nano* **2013**, *7*, 9318−9324.
(7) Shao, S. F.; Qiu, X. M.; He, D. F.; Koehn, R.; Guan, N. J.; Lu, X. H.; Bao, N. Z.; Grimes, C. A. Low Temperature Crystallization of Transparent, Highly Ordered Nanoporous SnO_2 Thin Films: Application to Room-temperature Hydrogen Sensing. *Nanoscale* **2011**, *3*, 4283−4289.
(8) Song, L. M.; Zhang, S. J.; Chen, B.; Ge, J. J.; Jia, X. C. A Hydrothermal Method for Preparation of alpha-Fe_2O_3 Nanotubes and Their Catalytic Performance for Thermal Decomposition of Ammonium Perchlorate. *Colloids Surf., A* **2010**, *360*, 1−5.
(9) Chen, J.; Xu, L. N.; Li, W. Y.; Gou, X. L. Alpha-Fe_2O_3 Nanotubes in Gas Sensor and Lithium-ion Battery Applications. *Adv. Mater.* **2005**, *17*, 582.
(10) Burleigh, T. D.; Schmuki, P.; Virtanen, S. Properties of the Nanoporous Anodic Oxide Electrochemically Grown on Steel in Hot 50% NaOH. *J. Electrochem. Soc.* **2009**, *156*, C45−C53.
(11) Mor, G. K.; Varghese, O. K.; Paulose, M.; Grimes, C. A. Transparent Highly Ordered TiO_2 Nanotube Arrays via Anodization of Titanium Thin Films. *Adv. Funct. Mater.* **2005**, *15*, 1291−1296.
(12) Mohapatra, S. K.; John, S. E.; Banerjee, S.; Misra, M. Water Photooxidation by Smooth and Ultrathin alpha-Fe_2O_3 Nanotube Arrays. *Chem. Mater.* **2009**, *21*, 3048−3055.
(13) Xie, K. Y.; Li, J.; Lai, Y. Q.; Lu, W.; Zhang, Z. A.; Liu, Y. X.; Zhou, L. M.; Huang, H. T. Highly Ordered Iron Oxide Nanotube Arrays as Electrodes for Electrochemical Energy Storage. *Electrochem. Commun.* **2011**, *13*, 657−660.
(14) Wang, C. J.; Sahay, P. Breath Analysis Using Laser Spectroscopic Techniques: Breath Biomarkers, Spectral Fingerprints, and Detection Limits. *Sensors* **2009**, *9*, 8230−8262.
(15) Righettoni, M.; Tricoli, A.; Pratsinis, S. E. Si:WO_3 Sensors for Highly Selective Detection of Acetone for Easy Diagnosis of Diabetes by Breath Analysis. *Anal. Chem.* **2010**, *82*, 3581−3587.
(16) Feng, P.; Wan, Q.; Wang, T. H. Contact-Controlled Sensing Properties of Flowerlike ZnO Nanostructures. *Appl. Phys. Lett.* **2005**, *87*, 21.
(17) Tao, Y. R.; Gao, Q. X.; Di, J. L.; Wu, X. C. Gas Sensors Based on alpha-Fe_2O_3 Nanorods, Nanotubes and Nanocubes. *J. Nanosci. Nanotechnol.* **2013**, *13*, 5654−5660.
(18) Kim, H. J.; Choi, K. I.; Pan, A. Q.; Kim, I. D.; Kim, H. R.; Kim, K. M.; Na, C. W.; Cao, G. Z.; Lee, J. H. Template-free Solvothermal Synthesis of Hollow Hematite Spheres and Their Aapplications in Gas sensors and Li-ion Batteries. *J. Mater. Chem.* **2011**, *21*, 6549−6555.
(19) Su, D. W.; Kim, H. S.; Kim, W. S.; Wang, G. X. Synthesis of Tuneable Porous Hematites (alpha-Fe_2O_3) for Gas Sensing and Lithium Storage in Lithium Ion Batteries. *Micropor. Mesopor. Mater.* **2012**, *149*, 36−45.
(20) Chen, H. M.; Zhao, Y. Q.; Yang, M. Q.; He, J. H.; Chu, P. K.; Zhang, J.; Wu, S. H. Glycine-assisted Hydrothermal Synthesis of Peculiar Porous alpha-Fe_2O_3 Nanospheres with Excellent Gas-sensing Properties. *Anal. Chim. Acta* **2010**, *659*, 266−273.
(21) Fang, X. L.; Chen, C.; Jin, M. S.; Kuang, Q.; Xie, Z. X.; Xie, S. Y.; Huang, R. B.; Zheng, L. S. Single-crystal-like Hematite Colloidal Nanocrystal Clusters: Synthesis and Applications in Gas Sensors, Photocatalysis and Water Treatment. *J. Mater. Chem.* **2009**, *19*, 6154−6160.
(22) Cao, Y. L.; Luo, H. Y.; Jia, D. Z. Low-heating Solid-state Synthesis and Excellent Gas-sensing Properties of alpha-Fe_2O_3 Nanoparticles. *Sens. Actuators, B* **2013**, *176*, 618−624.
(23) Sun, P.; Du, S. S.; Yang, T. L.; Li, X. W.; Liu, F. M.; Liang, X. S.; Gao, Y.; Sun, Y. F.; Lu, G. Y. Controlled Synthesis of Hierarchical Sn-doped alpha-Fe_2O_3 with Novel Sheaf-like Architectures and Their Gas Sensing Properties. *RSC Adv.* **2013**, *3*, 7112−7118.
(24) Song, H. J.; Jia, X. H.; Zhang, X. Q. Controllable Fabrication, Growth Mechanism, and Gas Sensing Properties of Hollow Hematite Polyhedra. *J. Mater. Chem.* **2012**, *22*, 22699−22705.
(25) Gunawan, P.; Mei, L.; Teo, J.; Ma, J. M.; Highfield, J.; Li, Q. H.; Zhong, Z. Y. Ultrahigh Sensitivity of Au/1D alpha-Fe_2O_3 to Acetone and the Sensing Mechanism. *Langmuir* **2012**, *28*, 14090−14099.
(26) Sun, P.; Wang, W. N.; Liu, Y. P.; Sun, Y. F.; Ma, J.; Lu, G. Y. Hydrothermal Synthesis of 3D Urchin-like alpha-Fe_2O_3 Nanostructure for Gas Sensor. *Sens. Actuators, B* **2012**, *173*, 52−57.
(27) Dou, Z. F.; Cao, C. Y.; Wang, Q.; Qu, J.; Yu, Y.; Song, W. G. Synthesis, Self-Assembly, and High Performance in Gas Sensing of X-Shaped Iron Oxide Crystals. *ACS Appl. Mater. Interfaces* **2012**, *4*, 5698−5703.
(28) Liu, X. J.; Chang, Z.; Luo, L.; Lei, X. D.; Liu, J. F.; Sun, X. M. Sea Urchin-like Ag-alpha-Fe_2O_3 Nanocomposite Microspheres: Synthesis and Gas Sensing Applications. *J. Mater. Chem.* **2012**, *22*, 7232−7238.
(29) Song, H. J.; Jia, X. H.; Qi, H.; Yang, X. F.; Tang, H.; Min, C. Y. Flexible Morphology-Controlled Synthesis of Monodisperse alpha-Fe_2O_3 Hierarchical Hollow Microspheres and Their Gas-sensing Properties. *J. Mater. Chem.* **2012**, *22*, 3508−3516.
(30) Sun, P.; You, L.; Wang, D. W.; Sun, Y. F.; Ma, J.; Lu, G. Y. Synthesis and Gas Sensing Properties of Bundle-like alpha-Fe_2O_3 Nanorods. *Sens. Actuators, B* **2011**, *156*, 368−374.
(31) Xia, Y. S.; Dai, H. X.; Jiang, H. Y.; Zhang, L.; Deng, J. G.; Liu, Y. X. Three-dimensionally Ordered and Wormhole-like Mesoporous Iron Oxide Catalysts Highly Active for the Oxidation of Acetone and Methanol. *J. Hazard. Mater.* **2011**, *186*, 84−91.
(32) Picasso, G.; Quintilla, A.; Pina, M. P.; Herguido, J. Total Combustion of Methyl-ethyl Ketone over Fe_2O_3 Based Catalytic Membrane Reactors. *Appl. Catal., B* **2003**, *46*, 133−143.
(33) Li, J.; Lu, Y. J.; Ye, Q.; Cinke, M.; Han, J.; Meyyappan, M. Carbon Nanotube Sensors for Gas and Organic Vapor Detection. *Nano Lett.* **2003**, *3*, 929−933.